

Atomically Resolved Electronic States and Correlated Magnetic Order at Termination Engineered Complex Oxide Heterointerfaces

Bo-Chao Huang,^{†,§} Pu Yu,^{*,‡,⊗} Y. H. Chu,^{§,||} Chia-Seng Chang,[§] Ramamoorthy Ramesh,[⊥] Rafal E. Dunin-Borkowski,[#] Philipp Ebert,^{#,Ⓛ} and Ya-Ping Chiu^{*,†,§,Ⓛ}

[†]Department of Physics, National Taiwan University, Taipei 106, Taiwan

[‡]State Key Laboratory of Low-Dimensional Quantum Physics, Department of Physics, Tsinghua University, and Collaborative Innovation Center of Quantum Matter, Beijing 100084, China

[§]Institute of Physics, Academia Sinica, Taipei 105, Taiwan

^{||}Department of Materials Science and Engineering, National Chiao Tung University, Hsinchu 300, Taiwan

[⊥]Department of Physics, University of California, Berkeley, California 94720, United States

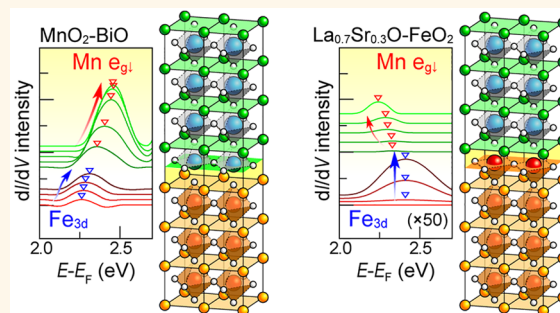
[#]Peter Grünberg Institut, Forschungszentrum Jülich GmbH, 52425 Jülich, Germany

[⊗]RIKEN Center for Emergent Matter Science (CEMS), Wako, Saitama 351-0198, Japan

Supporting Information

ABSTRACT: We map electronic states, band gaps, and interface-bound charges at termination-engineered $\text{BiFeO}_3/\text{La}_{0.7}\text{Sr}_{0.3}\text{MnO}_3$ interfaces using atomically resolved cross-sectional scanning tunneling microscopy. We identify a delicate interplay of different correlated physical effects and relate these to the ferroelectric and magnetic interface properties tuned by engineering the atomic layer stacking sequence at the interfaces. This study highlights the importance of a direct atomically resolved access to electronic interface states for understanding the intriguing interface properties in complex oxides.

KEYWORDS: complex oxide heterointerfaces, BiFeO_3 , $\text{La}_{0.7}\text{Sr}_{0.3}\text{MnO}_3$, cross-sectional scanning tunneling microscopy, atomically resolved electronic states



Complex oxide heterointerfaces exhibit intriguing physical phenomena arising from the presence of multiple degrees of freedom, namely spin, charge, orbital character, and lattice structure, as well as their mutual correlation. Recently, improvements in growth and characterization techniques have provided the opportunity to manipulate the coupling of 3d electrons, leading to a rich variety of physical phenomena. For example, two-dimensional electron gases were found at junctions between two insulators¹ and metallic ferromagnetic states have been reported to occur between antiferromagnetic insulators.² Achieving a detailed physical understanding of such exotic phenomena will lead to the ability to control and tune desired properties, making complex oxide materials highly attractive for next-generation electronic and spintronic devices.^{3,4}

A particularly interesting system is the antiferromagnetic insulator BiFeO_3 (BFO)–ferromagnetic metal $\text{La}_{0.7}\text{Sr}_{0.3}\text{MnO}_3$ (LSMO) heterojunction, which combines a multiferroic material and a colossal magnetoresistive material. By tuning

the atomic termination at the interface with layer-by-layer precision, the ferroelectric polarization can be manipulated^{5–7} and simultaneously the magnetic order is expected to change from ferro- to anti-ferromagnetic.⁸ However, the physical origin of these phenomena is still unclear and under debate. On the one hand, orbital reconstruction at the interface^{9,10} has been suggested to govern interface magnetism and to induce magnetoelectric coupling.¹¹ On the other hand, an alternative theory predicts charge transfer between the LSMO and BFO layers, which activates double- and superexchange mechanisms between adjacent atomic layers across the interface, resulting in an electric-field (or ferroelectric polarization) tunable interfacial magnetic state.¹² However, the search for a single physical origin may neglect the possibility of a delicate interplay of

Received: August 22, 2017

Accepted: January 22, 2018

Published: January 31, 2018

different correlated processes including orbital, charge, and magnetic ordering as well as lattice degrees of freedom.¹³

Furthermore, the experimental basis lacks an atomically resolved spectroscopic view of the electronic states near the Fermi energy (E_F) localized directly at interface. Disentangling the physical origins of the interface properties requires, however, such data to identify the electronic interface states, their occupation and the resulting bound charges, ferroelectric polarization, changes of the oxidation states, and correlation with magnetic properties. Only with such detailed high-resolution experimental data it will be possible to explore the relevance of the different physical models.^{14–18}

Therefore, we apply cross-sectional scanning tunneling microscopy (STM) and spectroscopy (STS) to probe directly the electronic states and charges with atomic precision right at and across complex oxide interfaces. With this technique we probe the electronic properties localized directly at BFO/LSMO heterointerfaces, revealing the underlying physical mechanisms and interfaces' magnetic ordering. This forms the basis for an atomic-scale physical understanding of complex oxide heterointerface properties, which is central for designing complex oxide heterointerface properties, which is central for designing complex oxide devices.

RESULTS AND DISCUSSION

In order to address the effect of different layer terminations (or stacking sequences) at the interface, two types of 50 nm BFO on 5 nm LSMO heterostructures were grown on Nb-doped TiO_2 -terminated SrTiO_3 (001) (STO) substrates. The first one had a layer stacking sequence at the interface of $\text{La}_{0.7}\text{Sr}_{0.3}\text{O}-\text{MnO}_2-\text{BiO}-\text{FeO}_2$ (*i.e.*, a MnO_2-BiO terminated LSMO/BFO interface, Figure 1a). The layer termination of the second

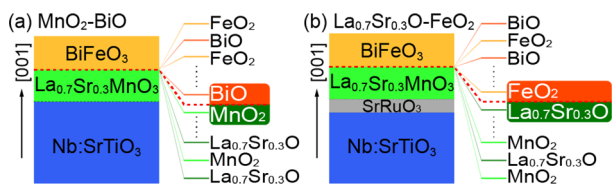


Figure 1. Schematic diagram of two possible atomic-stacking sequences for LSMO/BFO heterostructures with (a) MnO_2-BiO , and (b) $\text{La}_{0.7}\text{Sr}_{0.3}\text{O}-\text{FeO}_2$ layer termination at the interfaces.

sample was tuned by inserting 1.5 unit cells of SrRuO_3 , *i.e.*, a $\text{SrO}-\text{RuO}_2-\text{SrO}$ sequence, between the STO substrate and the LSMO layer.⁵ The resulting stacking sequence at the interface is $\text{MnO}_2-\text{La}_{0.7}\text{Sr}_{0.3}\text{O}-\text{FeO}_2-\text{BiO}$ (*i.e.*, a $\text{La}_{0.7}\text{Sr}_{0.3}\text{O}-\text{FeO}_2$ terminated interface, Figure 1b).^{5,7,19} The Curie temperature (T_c) of the 5 nm $\text{La}_{0.7}\text{Sr}_{0.3}\text{MnO}_3$ ultrathin film is about 320 K for the MnO_2-BiO and 300 K for the $\text{La}_{0.7}\text{Sr}_{0.3}\text{O}-\text{FeO}_2$, which can be referred in our previous works.^{11,20}

For our STM and STS studies, we cleaved cross sections through both types of heterostructures *in situ* in ultrahigh vacuum (7×10^{-11} mbar). The cleavage exposes (100) cross-sectional planes through the whole heterostructures, which were investigated by STM at 80 K (below the Curie temperature) using tungsten tips. Figure 2(a) illustrates the morphology of the (100) cleavage surface of the $\text{BiFeO}_3/\text{La}_{0.7}\text{Sr}_{0.3}\text{MnO}_3/\text{SrTiO}_3$ heterostructure measured by STM. The Nb-doped STO substrate exhibits large atomically smooth terraces separated by monolayer (0.4 nm) high steps as visible in the height histogram shown in the Supporting Information.²¹ The LSMO layer appears brighter (higher topography), again

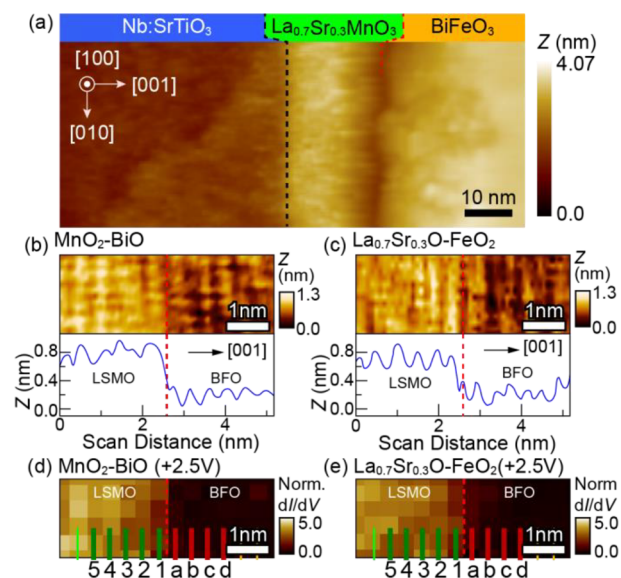


Figure 2. (a) Constant-current cross-sectional STM image showing an overview of the heterostructure consisting of the Nb-doped SrTiO_3 substrate, the $\text{La}_{0.7}\text{Sr}_{0.3}\text{MnO}_3$ layer, and the BiFeO_3 layer (from left to right). The image was acquired at a set point of -0.5 V and 50 pA. Atomically resolved STM images of the (b) MnO_2-BiO and (c) $\text{La}_{0.7}\text{Sr}_{0.3}\text{O}-\text{FeO}_2$ terminated interfaces (set points: $V = +3$ V and $I = 200$ pA). The height profile below exhibits a periodicity of ~ 0.4 nm, in line with the bulk lattice constant. (d) and (e) Normalized differential conductivity maps of the same areas as in (b) and (c), respectively. The dashed red lines are used to identify the interface location.

with smooth terraces. The contrast change between the STO substrate and the LSMO layer is abrupt and straight. No interface roughness is observed, indicating an atomically precise layer stacking. The BFO cleavage surface is rougher than the two previous materials. It exhibits a high density of 0.4 nm steps, corresponding to a FeO_2-BiO layer pair (see Supporting Information). The increased roughness can be attributed to the spontaneous polarization in $[111]$ direction of the $R3c$ phase of BFO, resulting in a weak polar character of its (100) planes, reducing the cleavability. The interface between LSMO and BFO appears as a dark line (marked by the red dashed line) and exhibits a few kinks, indicating a slightly rough LSMO growth surface. However, we note that these features do not affect the stacking sequence at the interface, which was predesigned during growth.

Parts b and c of Figure 2 show atomically resolved STM images of the MnO_2-BiO - and $\text{La}_{0.7}\text{Sr}_{0.3}\text{O}-\text{FeO}_2$ -terminated interfaces, respectively. Average height profiles shown below Figure 2b,c display a 0.4 nm periodicity, in agreement with the bulklike surface periodicity.¹⁹ Indeed, the most favorable termination of the $\text{La}_{0.7}\text{Sr}_{0.3}\text{MnO}_3$ (100) cleavage surface is a bulklike MnO_2 (100) layer,^{22,23} while BiFeO_3 (100) surfaces are bulklike FeO_2 terminated.^{8,24}

For identifying the interface position, we turn to spectroscopic measurements, which reveal distinct changes in electronic properties between LSMO and BFO. Parts d and e of Figure 2 show normalized differential conductivity $[(dI/dV)/(I/V)]$ images measured at +2.5 V with 0.4 nm spatial resolution across the MnO_2-BiO - and $\text{La}_{0.7}\text{Sr}_{0.3}\text{O}-\text{FeO}_2$ -terminated interfaces, respectively. A pronounced change in the $(dI/dV)/(I/V)$ signal is observable, due to different band structures and hence densities of states between the two

materials. The interface is identified as the position of the steepest change of the $(dI/dV)/(I/V)$ signal assuming that electronic and compositional properties follow each other.

In order to elucidate the evolution of the electronic structure across the two types of LSMO/BFO heterointerfaces, spatially resolved normalized differential conductivity spectra were measured at every pixel point. For each spectrum, the tip-sample separation was kept constant. All spectra recorded from a pixel line parallel to the interface were averaged as outlined in the Supporting Information. The averaged spectra have a spatial separation of 0.4 nm (one lattice constant) perpendicular to the interface. They are labeled using the same labels as for the pixel lines shown in Figure 2d,e. Parts a and b of Figure 3 show the

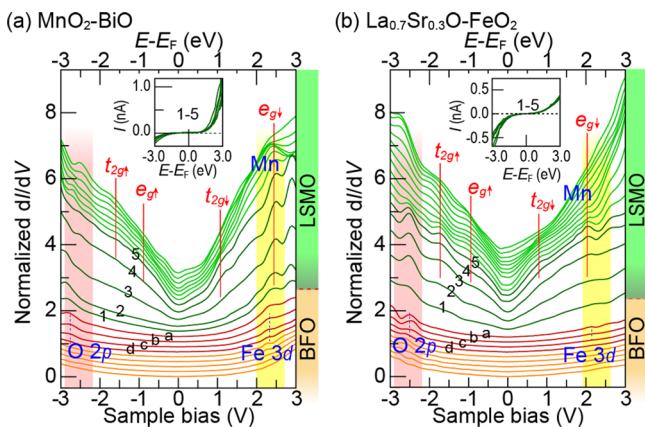


Figure 3. Spatial evolution across the (a) $\text{MnO}_2\text{-BiO}$ and (b) $\text{La}_{0.7}\text{Sr}_{0.3}\text{O-FeO}_2$ terminated interfaces of the normalized dI/dV in atomic layer steps. Successive spectra are offset vertically for clarity. The light and dark green spectra on the LSMO side are labeled by numbers, whereas those on the BFO side (red and orange) have letters as labels. The different features discussed in the text are marked by vertical (dashed) lines and labeled O 2p, (Mn) t_{2g} , (Mn) e_{g1} , (Mn) t_{2g1} , (Mn) e_{g1} , and Fe 3d.

resulting layer-by-layer-resolved normalized differential conductivity spectra plotted as a function of sample bias across the $\text{MnO}_2\text{-BiO}$ - and $\text{La}_{0.7}\text{Sr}_{0.3}\text{O-FeO}_2$ -terminated interfaces, respectively.

The spectra of the BFO surface exhibit a semiconducting behavior with negligible tunnel current over a wide energy range.^{8,25} In contrast, the LSMO surface is metallic, with only a dip in the density of states $[(dI/dV)/(I/V)]$ near the Fermi energy (at 0 V).²⁶

The tunneling spectra exhibit pronounced asymmetries between the current recorded at positive and negative sample voltages. The insets in Figure 3a (and b) show that the tunnel current is larger at positive (negative) voltages for the $\text{MnO}_2\text{-BiO}$ ($\text{La}_{0.7}\text{Sr}_{0.3}\text{O-FeO}_2$)-terminated interfaces. In analogy to p-n junctions,²⁷ these characteristics show that the $\text{MnO}_2\text{-BiO}$ and $\text{La}_{0.7}\text{Sr}_{0.3}\text{O-FeO}_2$ terminated interfaces exhibit n-type and p-type characteristics, respectively. This indicates positive and negative bound charges localized at the $\text{MnO}_2\text{-BiO}$ - and $\text{La}_{0.7}\text{Sr}_{0.3}\text{O-FeO}_2$ -terminated interfaces, screened by free electrons (n-type) and holes (p-type), respectively, originating from the very high free carrier concentration in the metallic LSMO layer.²⁸

The opposite bound charge at the two differently terminated interfaces can be related directly to the discontinuity of the ferroelectric polarization in the BFO layer at the interface to the

metallic LSMO. Polarization pointing away from (toward) the BFO/LSMO interface induces a positive (negative) bound charge localized at the interface. Hence, the BFO layers in the two heterostructures exhibit opposite polarization, pointing away from the $\text{MnO}_2\text{-BiO}$ -terminated interface (*i.e.*, in $[001]$ growth direction) and toward the $\text{La}_{0.7}\text{Sr}_{0.3}\text{O-FeO}_2$ -terminated interface (in $[00\bar{1}]$ direction), in agreement with calculations.⁵

At this stage, we turn to the details of the electronic density of states near the Fermi energy. In addition to the general shape of the tunneling spectra discussed above, one can discern several additional features in the tunneling spectra in Figure 3. In the LSMO layer, the feature between 0 and -1 eV agrees well with the e_{g1} state of the Mn 3d orbital split by the crystal field (Mn e_{g1}), found experimentally and theoretically at 0 to -1.3 eV (relative to E_F).^{26,29,30} In analogy, the feature around -1.7 eV can be correlated with the t_{2g1} state of the split Mn 3d orbital (Mn t_{2g1}).^{26,29,30} The lowest energy peak at approximately -2.5 eV can be interpreted as the O 2p state.^{29,30} In the empty states of LSMO, the shoulder between $+1$ and $+1.5$ eV can be attributed to the Mn t_{2g1} state, whereas the feature at $+2$ to $+2.5$ eV can be correlated with the Mn e_{g1} state.^{30,31} In the BFO layer, the additional peak at $+2.3$ eV corresponds to the Fe 3d state.³² Some of the observed features may arise from surface states. However, angle-resolved photoelectron spectroscopy measurements of LSMO(100) surfaces found only three filled bulk states,^{33–35} in agreement with our tunneling spectra and our interpretation in terms of bulk states only.

We now discuss the evolution of the electronic structure across the LSMO/BFO interface. The frames in Figure 4a show

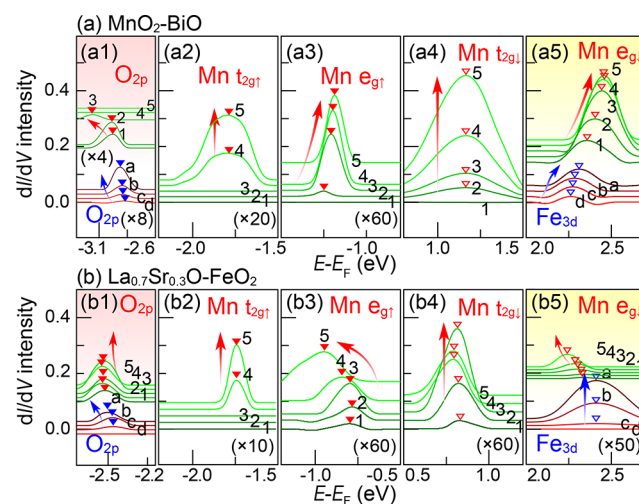


Figure 4. Layer-resolved spatial evolution of the different spectroscopic features observed in normalized dI/dV across the (a) $\text{MnO}_2\text{-BiO}$ and (b) $\text{La}_{0.7}\text{Sr}_{0.3}\text{O-FeO}_2$ terminated heterointerfaces. Successive spectra are offset vertically for clarity.

background-subtracted peaks of the occupied O 2p orbital and the Mn t_{2g1} and Mn e_{g1} states, as well as the empty Mn t_{2g1} and Mn e_{g1} states, and their evolution across the $\text{MnO}_2\text{-BiO}$ terminated interface (for the background subtraction, see the Supporting Information). Figure 4b illustrates corresponding electronic states across the $\text{La}_{0.7}\text{Sr}_{0.3}\text{O-FeO}_2$ terminated interface. Directly at the interface (spectra labeled 1 and a, for the $\text{MnO}_2\text{-BiO}$ and $\text{La}_{0.7}\text{Sr}_{0.3}\text{O-FeO}_2$ terminated interfaces), only two features are detectable. First, the unoccupied Mn 3d e_{g1} state on the LSMO side at about $+2.30$ eV above E_F overlaps with/evolves into the electronic peak associated with the

unoccupied Fe 3d_i state on the BFO side [Figure 4 (a5) and (b5), highlighted by the yellow bar in Figure 3]. Second, the O 2p peak at -2.5 V is prominent near the interface [Figure 4 (a1) and (b1), highlighted by the rose colored bar in Figure 3]. All of the other states are primarily on the LSMO sides of the interfaces.

Out of the states on the LSMO side, the Mn $t_{2g\downarrow}$ and $t_{2g\uparrow}$ states remain fixed in energy with increasing distance from both interfaces, while all other states shift in energy. The Mn 3d $e_{g\downarrow}$ and $e_{g\uparrow}$ states shift with increasing distance from MnO₂–BiO (La_{0.7}Sr_{0.3}O–FeO₂) terminated interfaces to higher (lower) energies. The O 2p states shift weakly to lower energies for both interfaces. Simultaneously the valence and conduction band edge positions shift, decreasing (increasing) the band gap within the BFO layer when approaching the MnO₂–BiO (La_{0.7}Sr_{0.3}O–FeO₂) terminated interface (Figure 5). At a distance of more than four lattice constants, the BFO bulk band gap of 2.9 eV is reached, which is close to the optical bulk band gap of 2.6 eV.³⁶

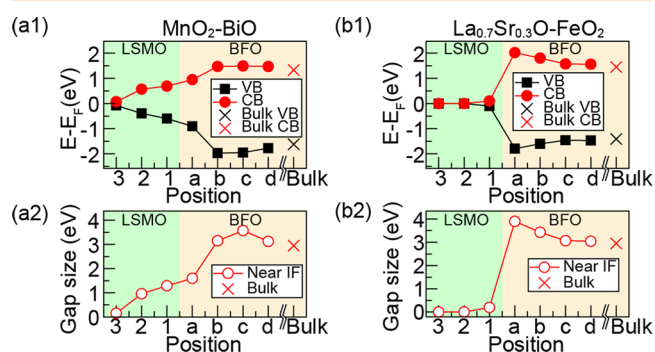


Figure 5. Conduction band (CB) and valence band (VB) edge positions (upper row) and band gap (lower row) extracted from tunneling spectra recorded from the MnO₂–BiO (left column, a1, and a2) and La_{0.7}Sr_{0.3}O–FeO₂ terminated (right column, b1, b2) interfaces. The crosses indicate bulk values far from any interfaces. The data are consistent with a semiconducting/insulating MnO₂–BiO interface and a metallic La_{0.7}Sr_{0.3}O–FeO₂-terminated interface, compatible with antiferromagnetic and ferromagnetic interface characteristics, respectively.

For the La_{0.7}Sr_{0.3}O–FeO₂-terminated interface, it should be noted that the metallic behavior of the LSMO layer starts directly at the interface position (Figure 5b), whereas the first two LSMO layers of the MnO₂–BiO terminated interface exhibit clear band gaps (Figure 5a). This observation is consistent with semiconducting (or insulating) and metallic characteristics of the MnO₂–BiO- and La_{0.7}Sr_{0.3}O–FeO₂-terminated interfaces, respectively.^{11,37}

We now discuss the interplay and correlation of the different physical properties observed at the interfaces. The energy shifts of the electronic states near E_F can be discussed on the basis of previously observed local distortions of the atomic lattice^{19,38} and general physical considerations as outlined below:

First, the lattice mismatch is only 0.5% in our system, and hence, no relevant epitaxial strain effects are observed, which is corroborated by the lack of interface misfit dislocations.^{39,40} Instead a slight distortion of the first three monolayers at the interface has been detected, which is related to tilts (or directional deformations) of the oxygen octahedra in the vicinity of the interface.^{5,19}

Second, the Mn 3d e_g states (but not the t_{2g} states) point toward the neighboring O atoms and are related to interatomic Mn–O bonds.⁴¹ Thus, Mn 3d e_g states exhibit a much larger Jahn–Teller activity, *i.e.*, larger energy shifts and splits with symmetry-lowering distortions, than the t_{2g} states, which do not shift significantly with lattice distortions.⁴² This agrees with our observations of large (small) shifts for Mn 3d e_g (t_{2g}) states.

In contrast, charge transfers or electrostatic fields can be excluded as the primary physical origin of the peak shifts, since they would shift all of the states close to E_F identically. Furthermore, the bound charges localized at the interfaces identified above are surrounded by screened Coulomb potentials, which give rise to a local band bending. However, the metallic LSMO layer screens the bound charges very effectively, such that the remaining band bending one lattice constant from the interfaces can be estimated to be below 10 meV.⁴³ This is not detectable in view of the much bigger shifts found. Hence, the bound charge is not responsible for the peak shifts.

The above discussion points to the importance of local distortions and tilts of the oxygen octahedral. In order to explore this and obtain deeper insight into the structural distortions and associated changes in orbital reconstruction, we examine the O 2p peak. The shift of the O 2p peak close to the interfaces suggests a different bonding structure of oxygen at the interfaces. In the bulk the oxygen octahedra surrounding Fe/Bi or Mn/Sr/La atoms are tilted. This distortion and the related tile pattern change at the interface.^{19,38}

(i) At the MnO₂–BiO-terminated interface, the tilt becomes zero, increasing toward the LSMO and BFO sides within three to five lattice constants to the bulk values.³⁸ The absence of a tilt at the interface is likely related to the fact that the MnO₂–BiO terminated interface is situated in the most rigid central square plane of the oxygen octahedra, where the stiff bonding is unable to accommodate changes in tilt between the two materials. The rigidity removes the tilt and the symmetry-lowering lattice distortion at the MnO₂–BiO-terminated interface, locally canceling the Jahn–Teller effect that is present in the bulk materials.⁴⁴ It is expected that this effect reduces the band gap,¹⁹ as we observed directly at the MnO₂–BiO terminated interface (Figure 5a, spatial position a).

The upward shifts of the two Mn 3d e_g states can therefore be interpreted as a signature of increasing tilt on the LSMO side. This behavior can be understood as follows. The distortion and the variation in rotation of the MnO₆ octahedra is closely connected to the oxidation state of Mn and hence to the Mn⁴⁺/Mn³⁺ ratio, since only Mn³⁺ (d⁴ ion) exhibits strong electron–lattice coupling.⁴⁵ Our LSMO material has mixed Mn oxidation states with 30% Mn⁴⁺ and 70% Mn³⁺ ions (on average d^{3.3} ions) in the bulk. The reduction of tilt and symmetry lowering distortions at the MnO₂–BiO-terminated interface³⁸ locally increases the Mn⁴⁺/Mn³⁺ ratio.^{19,46} On this basis and due to the sensitivity of the energy of Mn states on the oxidation state of Mn,⁴⁷ this replacement of Mn³⁺ by Mn⁴⁺ shifts the electronic states. Note, the change in oxidation state does not require a charge transfer with the bulk. Rather, the termination of the ferroelectric polarization at the interface provides the necessary charges by inducing a positive bound charge localized at the MnO₂–BiO terminated interface. This suggests that the bound charge is realized at the interface in form of a locally changed Mn oxidation state.

(ii) The La_{0.7}Sr_{0.3}O–FeO₂-terminated interface has a different structure, opposite bound charge, opposite energy shifts of

the Mn 3d $e_{g\downarrow}$ and 3d $e_{g\uparrow}$ states, and an opposite band gap opening, as compared to the MnO₂–BiO-terminated interface. The La_{0.7}Sr_{0.3}O–FeO₂-terminated interface is located at the tips of the oxygen octahedra, which are able to accommodate changes in octahedral rotation.³⁸ As a consequence, the La_{0.7}Sr_{0.3}O–FeO₂ terminated interface exhibits nonzero tilt, which differs considerably from that in the bulk material.³⁸ Hence, significant symmetry lowering lattice distortions are present at the La_{0.7}Sr_{0.3}O–FeO₂-terminated interface, in contrast to the MnO₂–BiO-terminated interface. When combined with compressive strain due to the lattice mismatch, the symmetry lowering lattice distortion widens the band gap due to the Jahn–Teller effect. Hence, our widened band gap is consistent with the presence of significant lattice distortions at the La_{0.7}Sr_{0.3}O–FeO₂-terminated interface.

The opposite energy shifts observed for the Mn 3d $e_{g\downarrow}$ and 3d $e_{g\uparrow}$ states indicate that the Mn⁴⁺/Mn³⁺ ratio decreases near the La_{0.7}Sr_{0.3}O–FeO₂-terminated interface, as found using electron energy-loss spectroscopy.^{19,46} The increased Mn³⁺ concentration induces a negative bound charge at the interface, as observed.

Finally, the different behavior of the band gaps and the shifts of the Mn 3d $e_{g\downarrow}$ and 3d $e_{g\uparrow}$ states, as well as the correlated changes of the Mn oxidation state, suggest the different magnetic properties of the two types of interface:

(i) The MnO₂–BiO terminated interface exhibits a wide band gap, *i.e.*, insulating properties, even within the first LSMO layers (Figure 5a). Furthermore, since the Mn oxidation state is intimately related to the spin of each Mn atom, a dominant Mn⁴⁺ oxidation state at the interface combined with insulating properties suggests an antiferromagnetic interface.³⁷

(ii) In contrast, the metallic behavior of the La_{0.7}Sr_{0.3}O–FeO₂-terminated interface (Figure 5b) is consistent with ferromagnetism due to a double exchange interaction, as present in metallic La_{0.7}Sr_{0.3}MnO₃ over a wide compositional range with mixed Mn oxidation states.¹¹ This hypothesis is corroborated by the observation of interface ferromagnetism at interfaces of reverse-grown La_{0.7}Sr_{0.3}MnO₃–BiFeO₃ on STO, which are expected to have the same La_{0.7}Sr_{0.3}O–FeO₂ layer termination.¹² The identification of antiferromagnetic and ferromagnetic MnO₂–BiO and La_{0.7}Sr_{0.3}O–FeO₂-terminated interfaces, respectively, agrees with theoretical calculations^{8,12} and is also corroborated by experimental results on manganite interfaces.^{11,37} Hence, at least for the manganite interfaces investigated here the correlation of the detailed electronic structure determination with magnetic ordering provides a fundamental insight into the physics of manganite complex oxide interfaces, critically important for future device applications.

CONCLUSIONS

In conclusion, we investigated the electronic properties of BiFeO₃–La_{0.7}Sr_{0.3}MnO₃ interfaces with different atomic stacking sequences, *i.e.*, MnO₂–BiO vs La_{0.7}Sr_{0.3}O–FeO₂. We mapped the spatial evolution of Mn, O, and Fe states across the interfaces with atomic precision using cross-sectional scanning tunneling spectroscopy. We derived a delicate interplay between the electronic states, band gaps, interface bound charges, screening charges, ferroelectric polarization, distortion-induced shifts, and changes of the oxidation state, leading to antiferromagnetic MnO₂–BiO and ferromagnetic La_{0.7}Sr_{0.3}O–FeO₂ terminated interfaces. The here presented direct experimental access to atomic-scale electronic properties right

at the complex oxide heterostructure interfaces provided an atomic-level understanding of the cross-correlation of the different degrees of freedom that are present at artificially constructed perovskite oxide heterointerfaces. Furthermore, achieving for manganite interfaces to connect such atomic-scale electronic properties with magnetic ordering eventually allows tailoring of their electronic and magnetic properties for future devices.

EXPERIMENTAL METHODS

Two types of La_{0.7}Sr_{0.3}MnO₃/BiFeO₃ heterostructures were grown on Nb-doped TiO₂-terminated SrTiO₃ (001) substrates. The first sample had a layer stacking sequence at the interface of La_{0.7}Sr_{0.3}O–MnO₂–BiO–FeO₂. The layer termination of the second sample was MnO₂–La_{0.7}Sr_{0.3}O–FeO₂–BiO.^{5,7,19}

Both types of heterostructures were then transferred to an ultrahigh vacuum STM chamber (7×10^{-11} mbar) and cleaved in situ at 80 K to obtain the cross-sectional slice of the Nb–SrTiO₃/La_{0.7}Sr_{0.3}MnO₃/BiFeO₃ heterostructures.

The scanning tunneling spectra (STS) were acquired at 80 K by using the current imaging tunneling spectroscopy (CITS) mode, where a series of tunnel current images was obtained at different sample bias voltage V_s . In this work, V_s was varied from +3.5 V to –3.5 V for STS measurements.

ASSOCIATED CONTENT

Supporting Information

The Supporting Information is available free of charge on the ACS Publications website at DOI: 10.1021/acsnano.7b06004.

Height histograms of the cleavage planes of the different materials/layers, averaging procedure of scanning tunneling spectra, and physical origin and subtraction procedure of the background in STS spectra (PDF)

AUTHOR INFORMATION

Corresponding Authors

*E-mail: ypchiu66@ntu.edu.tw.

*E-mail: yupu@mail.tsinghua.edu.cn.

ORCID

Philipp Ebert: 0000-0002-2022-2378

Ya-Ping Chiu: 0000-0001-7065-4411

Notes

The authors declare no competing financial interest.

ACKNOWLEDGMENTS

We thank the Ministry of Science and Technology of Taiwan (Contract No. MOST 103-2112-M-003-013-MY3, 104-2112-M-003-015-MY3, and 103-2119-M-009-003-MY3), the Ministry of Education of Taiwan (MOE-ATU 101W961), the National Basic Research Program of China (2015CB921700) and NSF China (11274194), and the European Research Council under the European Union's Seventh Framework Programme (Grant No. 320832) for financial support.

REFERENCES

- Ohtomo, A.; Hwang, H. Y. A High-mobility Electron Gas at the LaAlO₃/SrTiO₃ Heterointerface. *Nature* 2004, 427, 423–426.
- Bhattacharya, A.; May, S. J.; te Velthuis, S. G. E.; Warusawithana, M.; Zhai, X.; Jiang, B.; Zuo, J. M.; Fitzsimmons, M. R.; Bader, S. D.; Eckstein, J. N. Metal-Insulator Transition and Its Relation to Magnetic Structure in (LaMnO₃)_{2n}/(SrMnO₃)_n Superlattices. *Phys. Rev. Lett.* 2008, 100, 257203.

- (3) Hwang, H. Y.; Iwasa, Y.; Kawasaki, M.; Keimer, B.; Nagaosa, N.; Tokura, Y. Emergent Phenomena at Oxide Interfaces. *Nat. Mater.* **2012**, *11*, 103–113.
- (4) Zubko, P.; Gariglio, S.; Gabay, M.; Ghosez, P.; Triscone, J.-M. Interface Physics in Complex Oxide Heterostructures. *Annu. Rev. Condens. Matter Phys.* **2011**, *2*, 141–165.
- (5) Yu, P.; Luo, W.; Yi, D.; Zhang, J. X.; Rossell, M. D.; Yang, C. H.; You, L.; Singh-Bhalla, G.; Yang, S. Y.; He, Q.; Ramasse, Q. M.; Erni, R.; Martin, L. W.; Chu, Y. H.; Pantelides, S. T.; Pennycook, S. J.; Ramesh, R. Interface Control of Bulk Ferroelectric Polarization. *Proc. Natl. Acad. Sci. U. S. A.* **2012**, *109*, 9710–9715.
- (6) Wu, S. M.; Cybart, S. A.; Yu, P.; Rossell, M. D.; Zhang, J. X.; Ramesh, R.; Dynes, R. C. Reversible Electric Control of Exchange Bias in a Multiferroic Field-Effect Device. *Nat. Mater.* **2010**, *9*, 756–761.
- (7) Yu, P.; Chu, Y.-H.; Ramesh, R. Oxide Interfaces: Pathways to Novel Phenomena. *Mater. Today* **2012**, *15*, 320–327.
- (8) Jilili, J.; Eckern, U.; Schwingschlögl, U. Half-metallicity in a $\text{BiFeO}_3/\text{La}_{2/3}\text{Sr}_{1/3}\text{MnO}_3$ Superlattice: A First-Principles Study. *Europhys. Lett.* **2013**, *102*, 67009.
- (9) Benckiser, E.; Haverkort, M. W.; Brück, S.; Goering, E.; Macke, S.; Frañó, A.; Yang, X.; Andersen, O. K.; Cristiani, G.; Habermeier, H.-U.; Boris, A. V.; Zegkinoglou, I.; Wochner, P.; Hinkov, V.; Keimer, B. Orbital Reflectometry of Oxide Heterostructures. *Nat. Mater.* **2011**, *10*, 189–193.
- (10) Chakhalian, J.; Freeland, J. W.; Habermeier, H.-U.; Cristiani, G.; Khaliullin, G.; van Veenendaal, M.; Keimer, B. Orbital Reconstruction and Covalent Bonding at an Oxide Interface. *Science* **2007**, *318*, 1114–1117.
- (11) Yu, P.; Lee, J. S.; Okamoto, S.; Rossell, M. D.; Huijben, M.; Yang, C. H.; He, Q.; Zhang, J. X.; Yang, S. Y.; Lee, M. J.; Ramasse, Q. M.; Erni, R.; Chu, Y. H.; Arena, D. A.; Kao, C. C.; Martin, L. W.; Ramesh, R. Interface Ferromagnetism and Orbital Reconstruction in $\text{BiFeO}_3\text{-La}_{0.7}\text{Sr}_{0.3}\text{MnO}_3$ Heterostructures. *Phys. Rev. Lett.* **2010**, *105*, 027201.
- (12) Calderón, M. J.; Liang, S.; Yu, R.; Salafranca, J.; Dong, S.; Yunoki, S.; Brey, L.; Moreo, A.; Dagotto, E. Magnetolectric Coupling at the Interface of $\text{BiFeO}_3/\text{La}_{0.7}\text{Sr}_{0.3}\text{MnO}_3$ Multilayers. *Phys. Rev. B: Condens. Matter Mater. Phys.* **2011**, *84*, 024422.
- (13) Zimmermann, M. v.; Hill, J. P.; Gibbs, D.; Blume, M.; Casa, D.; Keimer, B.; Murakami, Y.; Tomioka, Y.; Tokura, Y. Interplay Between Charge, Orbital, and Magnetic Order in $\text{Pr}_{1-x}\text{Ca}_x\text{MnO}_3$. *Phys. Rev. Lett.* **1999**, *83*, 4872–4875.
- (14) Huang, B.-C.; Chiu, Y.-P.; Huang, P.-C.; Wang, W.-C.; Tra, V. T.; Yang, J.-C.; He, Q.; Lin, J.-Y.; Chang, C.-S.; Chu, Y.-H. Mapping Band Alignment across Complex Oxide Heterointerfaces. *Phys. Rev. Lett.* **2012**, *109*, 246807.
- (15) Sitaputra, W.; Sivasdas, N.; Skowronski, M.; Xiao, D.; Feenstra, R. M. Oxygen Vacancies on SrO-terminated $\text{SrTiO}_3(001)$ Surfaces Studied by Scanning Tunneling Spectroscopy. *Phys. Rev. B: Condens. Matter Mater. Phys.* **2015**, *91*, 205408.
- (16) Chien, T. Y.; Liu, J.; Chakhalian, J.; Guisinger, N. P.; Freeland, J. W. Visualizing Nanoscale Electronic Band Alignment at the $\text{La}_{2/3}\text{Ca}_{1/3}\text{MnO}_3\text{Nb:SrTiO}_3$ Interface. *Phys. Rev. B: Condens. Matter Mater. Phys.* **2010**, *82*, 041101.
- (17) Shin, J.; Borisevich, A. Y.; Meunier, V.; Zhou, J.; Plummer, E. W.; Kalinin, S. V.; Baddorf, A. P. Oxygen-Induced Surface Reconstruction of SrRuO_3 and Its Effect on the BaTiO_3 Interface. *ACS Nano* **2010**, *4*, 4190–4196.
- (18) Kumar, A.; Arruda, T. M.; Kim, Y.; Ivanov, I. N.; Jesse, S.; Bark, C. W.; Bristowe, N. C.; Artacho, E.; Littlewood, P. B.; Eom, C.-B.; Kalinin, S. V. Probing Surface and Bulk Electrochemical Processes on the $\text{LaAlO}_3\text{-SrTiO}_3$ Interface. *ACS Nano* **2012**, *6*, 3841–3852.
- (19) Borisevich, A. Y.; Chang, H. J.; Huijben, M.; Oxley, M. P.; Okamoto, S.; Niranjana, M. K.; Burton, J. D.; Tsymbal, E. Y.; Chu, Y. H.; Yu, P.; Ramesh, R.; Kalinin, S. V.; Pennycook, S. J. Suppression of Octahedral Tilts and Associated Changes in Electronic Properties at Epitaxial Oxide Heterostructure Interfaces. *Phys. Rev. Lett.* **2010**, *105*, 087204.
- (20) Huijben, M.; Yu, P.; Martin, L. W.; Molegraaf, H. J. A.; Chu, Y. H.; Holcomb, M. B.; Balke, N.; Rijnders, G.; Ramesh, R. Ultrathin Limit of Exchange Bias Coupling at Oxide Multiferroic/Ferromagnetic Interfaces. *Adv. Mater.* **2013**, *25*, 4739–4745.
- (21) Sitaputra, W.; Skowronski, M.; Feenstra, R. M. Topographic and Electronic Structure of Cleaved $\text{SrTiO}_3(001)$ Surfaces. *J. Vac. Sci. Technol., A* **2015**, *33*, 031402.
- (22) Yoshimoto, M.; Maruta, H.; Ohnishi, T.; Sasaki, K.; Koinuma, H. *In Situ* Determination of the Terminating Layer of $\text{La}_{0.7}\text{Sr}_{0.3}\text{MnO}_3$ thin Films using Coaxial Impact-collision Ion Scattering Spectroscopy. *Appl. Phys. Lett.* **1998**, *73*, 187–189.
- (23) Loviat, F.; Rønnow, H. M.; Renner, C.; Aeppli, G.; Kimura, T.; Tokura, Y. The Surface Layer of Cleaved Bilayer Manganites. *Nanotechnology* **2007**, *18*, 044020.
- (24) Zheng, H.; Zhan, Q.; Zavaliche, F.; Sherburne, M.; Straub, F.; Cruz, M. P.; Chen, L.-Q.; Dahmen, U.; Ramesh, R. Controlling Self-Assembled Perovskite–Spinel Nanostructures. *Nano Lett.* **2006**, *6*, 1401–1407.
- (25) Higuchi, T.; Liu, Y.-S.; Yao, P.; Glans, P.-A.; Guo, J.; Chang, C.; Wu, Z.; Sakamoto, W.; Itoh, N.; Shimura, T.; Yogo, T.; Hattori, T. Electronic Structure of Multiferroic BiFeO_3 by Resonant Soft x-ray Emission Spectroscopy. *Phys. Rev. B: Condens. Matter Mater. Phys.* **2008**, *78*, 085106.
- (26) Park, J. H.; Vescovo, E.; Kim, H. J.; Kwon, C.; Ramesh, R.; Venkatesan, T. Direct Evidence for a Half-metallic Ferromagnet. *Nature* **1998**, *392*, 794–796.
- (27) Feenstra, R. M.; Yu, E. T.; Woodall, J. M.; Kirchner, P. D.; Lin, C. L.; Pettit, G. D. Cross-sectional Imaging and Spectroscopy of GaAs Doping Superlattices by Scanning Tunneling Microscopy. *Appl. Phys. Lett.* **1992**, *61*, 795–797.
- (28) Asamitsu, A.; Tokura, Y. Hall effect in $\text{La}_{1-x}\text{Sr}_x\text{MnO}_3$. *Phys. Rev. B: Condens. Matter Mater. Phys.* **1998**, *58*, 47–50.
- (29) de Jong, M. P.; Bergenti, I.; Osikowicz, W.; Friedlein, R.; Dediu, V. A.; Taliani, C.; Salaneck, W. R. Valence Electronic States Related to Mn^{2+} at $\text{La}_{0.7}\text{Sr}_{0.3}\text{MnO}_3$ Surfaces Characterized by Resonant Photoemission. *Phys. Rev. B: Condens. Matter Mater. Phys.* **2006**, *73*, 052403.
- (30) He, J.; Borisevich, A.; Kalinin, S. V.; Pennycook, S. J.; Pantelides, S. T. Control of Octahedral Tilts and Magnetic Properties of Perovskite Oxide Heterostructures by Substrate Symmetry. *Phys. Rev. Lett.* **2010**, *105*, 227203.
- (31) Pruneda, J. M.; Ferrari, V.; Rurali, R.; Littlewood, P. B.; Spaldin, N. A.; Artacho, E. Ferrodistortive Instability at the (001) Surface of Half-Metallic Manganites. *Phys. Rev. Lett.* **2007**, *99*, 226101.
- (32) Stroppa, A.; Picozzi, S. Hybrid Functional Study of Proper and Improper Multiferroics. *Phys. Chem. Chem. Phys.* **2010**, *12*, 5405–5416.
- (33) Chikamatsu, A.; Wadati, H.; Kumigashira, H.; Oshima, M.; Fujimori, A.; Hamada, N.; Ohnishi, T.; Lippmaa, M.; Ono, K.; Kawasaki, M.; Koinuma, H. Band Structure and Fermi Surface of $\text{La}_{0.6}\text{Sr}_{0.4}\text{MnO}_3$ Thin Films Studied by *In Situ* Angle-resolved Photoemission Spectroscopy. *Phys. Rev. B: Condens. Matter Mater. Phys.* **2006**, *73*, 195105.
- (34) Shi, M.; Falub, M. C.; Willmott, P. R.; Krempasky, J.; Herger, R.; Hricovini, K.; Patthey, L. κ -dependent Electronic Structure of the Colossal Magnetoresistive Perovskite $\text{La}_{0.66}\text{Sr}_{0.34}\text{MnO}_3$. *Phys. Rev. B: Condens. Matter Mater. Phys.* **2004**, *70*, 140407.
- (35) Krempaský, J.; Strocov, V. N.; Blaha, P.; Patthey, L.; Radović, M.; Falub, M.; Shi, M.; Hricovini, K. Bulk vs. Surface Effects in ARPES Experiment from $\text{La}_{2/3}\text{Sr}_{1/3}\text{MnO}_3$ Thin Films. *J. Electron Spectrosc. Relat. Phenom.* **2010**, *181*, 63–69.
- (36) Basu, S. R.; Martin, L. W.; Chu, Y. H.; Gajek, M.; Ramesh, R.; Rai, R. C.; Xu, X.; Musfeldt, J. L. Photoconductivity in BiFeO_3 Thin Film. *Appl. Phys. Lett.* **2008**, *92*, 091905.
- (37) Valencia, S.; Peña, L.; Konstantinovic, Z.; Balcells, L.; Galceran, R.; Schmitz, D.; Sandiumenge, F.; Casanove, M.; Martínez, B. Intrinsic Antiferromagnetic/insulating Phase at Manganite Surfaces and Interfaces. *J. Phys.: Condens. Matter* **2014**, *26*, 166001.
- (38) Kim, Y.-M.; Kumar, A.; Hatt, A.; Morozovska, A. N.; Tselev, A.; Biegalski, M. D.; Ivanov, I.; Eliseev, E. A.; Pennycook, S. J.; Rondinelli,

J. M.; Kalinin, S. V.; Borisevich, A. Y. Interplay of Octahedral Tilts and Polar Order in BiFeO₃ Films. *Adv. Mater.* **2013**, *25*, 2497–2504.

(39) Horiba, K.; Maniwa, A.; Chikamatsu, A.; Yoshimatsu, K.; Kumigashira, H.; Wadati, H.; Fujimori, A.; Ueda, S.; Yoshikawa, H.; Ikenaga, E.; Kim, J. J.; Kobayashi, K.; Oshima, M. Pressure-induced Change in the Electronic Structure of Epitaxially Strained La_{1-x}Sr_xMnO₃ Thin Films. *Phys. Rev. B: Condens. Matter Mater. Phys.* **2009**, *80*, 132406.

(40) Dholabhai, P. P.; Pilania, G.; Aguiar, J. A. Termination Chemistry-driven Dislocation Structure at SrTiO₃/MgO Hetero-interfaces. *Nat. Commun.* **2014**, *5*, 5043–5043.

(41) Tokura, Y.; Nagaosa, N. Orbital Physics in Transition-Metal Oxides. *Science* **2000**, *288*, 462–468.

(42) Saitoh, T.; Bocquet, A. E.; Mizokawa, T.; Namatame, H.; Fujimori, A.; Abbate, M.; Takeda, Y.; Takano, M. Electronic Structure of La_{1-x}Sr_xMnO₃ Studied by Photoemission and x-ray-absorption Spectroscopy. *Phys. Rev. B: Condens. Matter Mater. Phys.* **1995**, *51*, 13942–13951.

(43) Laubsch, A.; Urban, K.; Ebert, P. Three- to Two-dimensional Transition in Electrostatic Screening of Point Charges at Semiconductor Surfaces Studied by Scanning Tunneling Microscopy. *Phys. Rev. B: Condens. Matter Mater. Phys.* **2009**, *80*, 245314.

(44) Millis, A. J.; Darling, A. J. M. T.; Migliori, A. Quantifying Strain Dependence in “Colossal” Magnetoresistance Manganites. *J. Appl. Phys.* **1998**, *83*, 1588.

(45) Millis, A. J.; Littlewood, P. B.; Shraiman, B. I. Double Exchange Alone Does Not Explain the Resistivity of La_{1-x}Sr_xMnO₃. *Phys. Rev. Lett.* **1995**, *74*, 5144–5147.

(46) Kim, Y.-M.; Morozovska, A.; Eliseev, E.; Oxley, M. P.; Mishra, R.; Selbach, S. M.; Grande, T.; Pantelides, S. T.; Kalinin, S. V.; Borisevich, A. Y. Direct Observation of Ferroelectric Field Effect and Vacancy-controlled Screening at the BiFeO₃/LaxSr_{1-x}MnO₃ Interface. *Nat. Mater.* **2014**, *13*, 1019–1025.

(47) Kobayashi, S.; Tokuda, Y.; Mizoguchi, T.; Shibata, N.; Sato, Y.; Ikuhara, Y.; Yamamoto, T. Quantitative Analyses of Oxidation States for Cubic SrMnO₃ and Orthorhombic SrMnO_{2.5} with Electron Energy Loss Spectroscopy. *J. Appl. Phys.* **2010**, *108*, 124903.